Materials Today Advances 7 (2020) 100073

Contents lists available at ScienceDirect

Materials Today Advances

journal homepage: www.journals.elsevier.com/materials-today-advances/

Recent advances in gold-based metal enhanced fluorescence platforms for diagnosis and imaging in the near-infrared

C. Joyce, S.M. Fothergill, F. Xie*

Department of Materials, Imperial College London, Exhibition Road, London SW7 2AZ, UK

ARTICLE INFO

Article history:
Received 27 January 2020
Received in revised form
3 April 2020
Accepted 4 April 2020
Available online xxx

Keywords:
Fluorescence enhancement
Nanostructures
Biosensing
Bioimaging
NIR window

ABSTRACT

This review examines metal enhanced fluorescence (MEF) using gold (Au) nanostructures, with a focus on biomedical applications of this phenomenon, namely fluorescence biosensing and imaging. The mechanism by which MEF occurs will be briefly discussed before a thorough review of recent investigations, particularly surrounding cancer detection and imaging. Work in this field has primarily focused on substrate-based MEF and more recently has explored solution-based enhancement. Therefore, this review will examine both the different nanostructured substrates as well as the colloidal nanomaterials that have been synthesized, along with their interactions with fluorescent molecules. The potential applications of plasmonic probes for optical imaging, particularly in the near-infrared II (NIR-II) window, are also discussed. By incorporating MEF into diagnostic and imaging techniques, it is expected that there will be dramatic improvements to patient survival rates *via* early diagnosis and efficient treatment.

© 2020 The Authors. Published by Elsevier Ltd. This is an open access article under the CC BY-NC-ND license (http://creativecommons.org/licenses/by-nc-nd/4.0/).

1. Introduction

One- and two-dimensional plasmonic nanomaterials have become the focus of intensive research because of their unique physicochemical properties and their application in a number of research areas in the biomedical field, such as biosensing, bioimaging, and treatment [1–3]. Tailoring of the intrinsic scattering, absorption, and coupling properties of plasmonic nanostructures can greatly aid diagnosis and imaging techniques. For example, designing plasmonic nanostructures with high-scattering and low-absorption cross sections can enable the use of sensing and imaging platforms incorporating metal-enhanced fluorescence (MEF) [4] and surface-enhanced Raman scattering (SERS) [5], while the reverse, i.e. high-absorption and low-scattering cross sections facilitate therapeutic techniques such as photothermal [6] and photodynamic [7] therapies.

Gold (Au) in particular is considered to be one of the primary building blocks for the next generation of sensing, imaging, and therapeutic devices [8–10]. It is classed as a plasmonic material. Other examples include traditional metals such as silver [11], copper [12], and platinum [13] and non-traditional semiconductors such as titanium nitride [14] and copper sulfide [15]. Nanomaterials composed of Au have the ability, similar to all plasmonic nanomaterials, to confine and amplify light absorption and scattering within the volume of their nanostructure because of the localization and coupling of surface plasmons (an oscillating dipole of free electrons on the nanostructure's surface) with electromagnetic waves, called localized surface plasmon resonance (LSPR) (Fig. 1a) [16]. Moreover, these LSPRs are highly controllable as they are sensitive to features which influence the surface electron density, such as the structure shape, size, and dielectric constant (Fig. 1b) [17]. In addition to these optical properties of Au nanostructures, the ease at which their size and shape can be controlled [18], their facile surface modification [19], and biocompatibility [20] make them a preferred material to be used in the ultrasensitive detection and imaging techniques needed for the treatment of fatal diseases, such as cancer [20]. Cancer is a disease caused by the uncontrolled growth of cells and, according to the World Health Organization (WHO – www.who.int), was responsible for 9.6 million deaths in 2018. In this review, we summarize the advances in the design of Au plasmonic nanoprobes as a tool to significantly improve methods for cancer diagnosis and treatment, with a focus particularly on enhancing fluorescence-based diagnosis and imaging techniques.

* Corresponding author.
E-mail address: f.xie@imperial.ac.uk (F. Xie).

https://doi.org/10.1016/j.mtadv.2020.100073
2590-0498/© 2020 The Authors. Published by Elsevier Ltd. This is an open access article under the CC BY-NC-ND license (http://creativecommons.org/licenses/by-nc-nd/4.0/).

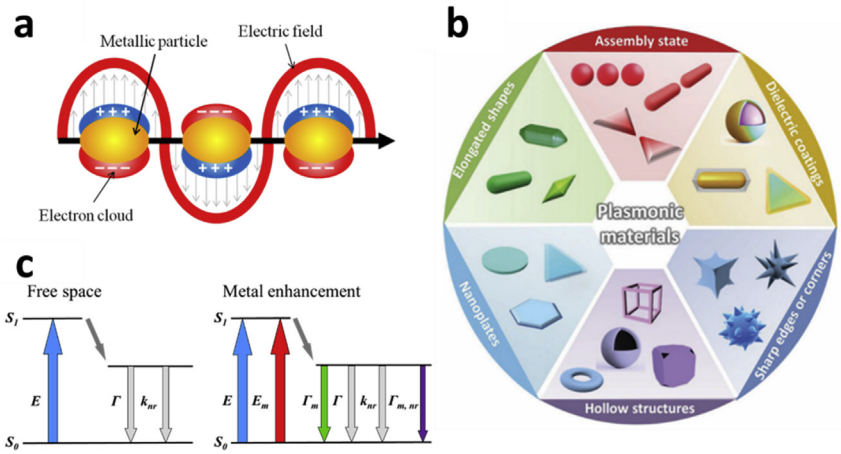


Fig. 1. (a) A representation of the localized surface plasmon resonance (LSPR) of a plasmonic nanomaterial induced by the irradiation of electromagnetic radiation. (b) An illustration depicting the vast array of metallic nanoparticle morphologies currently achievable – republished with permission of Royal Society of Chemistry, from the study by Zhu et al. [23] copyright (2014). (c) Jablonski diagram showing the pathways through which energy is transferred between energy states when a fluorophore is in the absence or presence of a metallic nanoparticle.

2. Metal-enhanced fluorescence

Before we review the variety of plasmonic nanostructures designed to improve a fluorophore's efficiency, it is first important to discuss how metallic nanomaterials can interact with a fluorophore through the process, that is, MEF. Once a fluorophore has been excited, one of two processes will then occur – the fluorophore will release its sudden excess energy in the form of a photon (light) or as a phonon (vibration), i.e. through either a radiative or non-radiative transition. The rates at which the radiative decay and non-radiative decay occur are denoted by the terms Γ and k_{nr}, respectively. It is these two rates of decay that determine both the quantum yield, Q, and lifetime, τ, of a fluorophore.

$$Q = \frac{\Gamma}{\Gamma + k_{nr}} \quad (1)$$

$$\tau = \frac{1}{\Gamma + k_{nr}} \quad (2)$$

The quantum yield (Eq. (1)) of a fluorophore, as previously stated, denotes its emission efficiency, while its fluorescence lifetime (Eq. (2)) is the length of time at which a fluorophore exists in the excited state before it returns to the ground state. When that same fluorophore is placed near a metallic surface or nanoparticle, the interaction between the two materials results in a modified quantum yield, Q_m, and lifetime, τ_m:

$$Q_m = \frac{\Gamma_0 + \Gamma_m}{\Gamma_0 + \Gamma_m + \Gamma_{m,nr} + k_{nr}} \quad (3)$$

$$\tau_m = \frac{1}{\Gamma_0 + \Gamma_m + \Gamma_{m,nr} + k_{nr}} \quad (4)$$

where Γ_m represents the modified radiative decay rate and $\Gamma_{m,nr}$ the additional non-radiative decay channels introduced by the presence of the metal nanoparticle (Fig. 1b) [21]. For a fluorophore to experience enhanced fluorescence, it must be placed within a 'sweet spot' distance from the metal nanoparticle (5–20 nm) [22]. It is at this distance that Γ_m becomes substantially large and $\Gamma_{m,nr}$ becomes insignificant, giving rise to enhanced fluorescence. Too close to the particle's surface, however, the $\Gamma_{m,nr}$ term dominates the equation and the fluorophore experiences quenching. Finally, if the fluorophore is held at a position too far from the particle, it does not experience the enhanced electric field and neither Γ_m nor $\Gamma_{m,nr}$ have any impact and the fluorophore acts as if it is in free space.

Explaining this in further detail, when a fluorophore is placed in proximity to a metal nanoparticle, the particle's effect on the fluorophore's emission intensity is twofold, as it modifies the rates of both the fluorophore's excitation and emission. As mentioned previously, metallic particles such as gold have an intrinsic, spectral property called LSPR. Therefore, exciting a particle at its LSPR wavelength leads to greatly amplified absorption and scattering of the particle. The increased scattering generates an enhanced near-field intensity of the electric field surrounding the particle which, if the fluorophore is placed within this near-field, increases its rate of excitation and results in higher fluorescence. Second, as the particle and fluorophore are in such close vicinity to each other, the plasmon band of the particle and the dipole of the excited fluorophore couple together, generating new pathways through which energy can pass. This coupling enables the non-radiative transfer of excitation energy from the particle to the fluorophore and also the transmission of the fluorophore's energy as radiation to the far field. This effect can be visually represented though a modified Jablonski diagram (Fig. 1c).

In both conditions (in the absence and presence of a metal nanoparticle), the fluorophore is excited by an electric field, E, from its ground state, S_0, to its excited state, S_1. In the presence of the particle, however, the fluorophore experiences an additional intensity of the electric field, E_m. In the free space condition, once the fluorophore is ready to relax to its ground state, it can only relax through either a radiative or a non-radiative pathway; however, in the presence of the metal nanoparticle, an additional radiative decay path, Γ_m, is created, allowing the fluorophore to emit a higher number of photons to phonons than previously possible and thus enhance the intensity of its fluorescence. This phenomenon can be exploited to greatly improve a number of fluorescence-based techniques used in the biomedical field, such as biosensing and fluorescence imaging.

3. Operating in the near-infrared

Many biomedical fluorescence-based techniques rely on using light in the UV-visible region of the electromagnetic spectrum. However, using this region can lead to certain disadvantages which

negatively impact the intensity of the fluorescent signal, resulting in indistinct readings or images. These signal-reducing processes occur as a result of the biological tissue itself and include absorption, scattering, and autofluorescence [24]. As such, there is significant interest in designing fluorescent dyes which both absorb and emit in the near-infrared I (NIR-I) and near-infrared II (NIR-II) windows [25] [–] [30] (650–900 nm and 1000–1700 nm, respectively), allowing improved imaging or sensing through biological media such as tissues or blood. The following paragraphs will detail the reasons for which NIR imaging can be used to overcome the signal-reducing phenomena.

Within biological tissue, many vital compounds, e.g. hemoglobin, melanins, reduced nicotinamide adenine dinucleotide (NADH), and amino acids such as tryptophan and phenylalanine, contain a conjugated π-bonding system [31,32]. Owing to their high degree of conjugation, these chromophores display intense absorption in the UV-visible end of the electromagnetic spectrum (<600 nm). Along with these compounds, water also contributes to the optical properties of biological tissue [33], with absorption particularly strong in the NIR region (~1450 nm). Considering the extinction spectra of all these light absorbers present in biological tissue, there exists a wavelength range (700–1700 nm) within which there is minimal light absorption of both excitation and fluorescence emission photons (Fig. 2a).

With regards to light scattering, a comprehensive study by Bashkatov et al. [34] on the optical properties of skin, subcutaneous tissue, and muscle showed an inversely proportional relationship between the amount of light scattered by the tissue and the wavelength of the excitation light. Therefore, to optimize the signal-to-noise ratio, it is necessary to use an NIR-II probe and light source, thus reducing the amount of scattering and giving clearer signals and sharper contrast.

Another phenomenon that inhibits the depth at which light can penetrate through tissue is autofluorescence. As mentioned earlier, biological tissue contains many chromophore molecules, such as flavins and NADH, which are capable of autofluorescence at wavelengths <600 nm. However, studies have shown that biological imaging using longer wavelength light induces a decreased level of tissue autofluorescence[35]. In fact, at wavelengths above 1500 nm, there is truly no autofluorescence, making imaging in this region a viable option for high signal-to-noise imaging [36].

As such, by shifting both the excitation and detection ranges for fluorescence imaging from the visible to the NIR, the processes that contribute to signal losses – scattering, absorption, autofluorescence, *etc.* –either are greatly reduced or become negligible. This results in a great improvement in the image resolution and depth penetration (Fig. 2b), which enables the definition of tissue structures previously unresolvable. It has been also shown that images taken in the NIR-II range, as compared even with the NIR-I range, have far superior resolution (micrometer resolution in comparison with millimeter) because of the further reduction in these signal-reducing phenomena [38,39]. A review by Hong et al. [24] contains a comprehensive list of dyes currently being investigated as potential NIR-I or NIR-II fluorescent biosensing and bioimaging probes, citing their excitation and emission wavelengths as well as their quantum yields. It should be noted that the majority of these NIR dyes listed have distinctly low quantum yields (<10%), meaning that a large amount of dye would be needed to produce a sufficiently bright signal which can be imaged without being lost to background autofluorescence and scattering. Therefore, to apply these dyes for use in ultrasensitive biosensing and real-time fluorescence imaging, their efficiency must be improved through the use of plasmonic nanostructures based on MEF.

4. MEF for biosensing

Early diagnosis of a disease is a crucial step in the treatment of a patient. Many diseases present such low biomarker concentrations during the early, treatable stages, that there is no biosensing technology sensitive enough to accurately diagnose patients until said disease has progressed to such an extent that it is oftentimes not possible to treat. One such example of this is pancreatic cancer. The 5-year survival rate of pancreatic cancer patients is 8%, because of the exceptional difficulty in detecting and intervening at the early stages of the disease [40]. Once finally diagnosed, most patients are unsuitable to undergo resection surgery as the disease has advanced to a point at which tumor resection is unlikely to provide any therapeutic benefit. There is a need, therefore, to design a system that can accurately detect disease to enable early intervention and ultimately, curing of the patient. One possible method through which this can be done is fluorescence biosensing [9,41,42].

Biosensors utilize biomolecules as recognition elements which are immobilized to a transducer. The recognition elements (e.g. antibodies, DNA, enzymes) can be selective to very specific disease biomarkers that are present in the body fluid, such as antigens including CA 19-9 [43] or CA-125 [44] for pancreatic cancer and ovarian cancer, respectively, or disease-specific micro-rnas [45]. The transducer converts the biological response, resulting from the interaction between the biomarker and the recognition element,

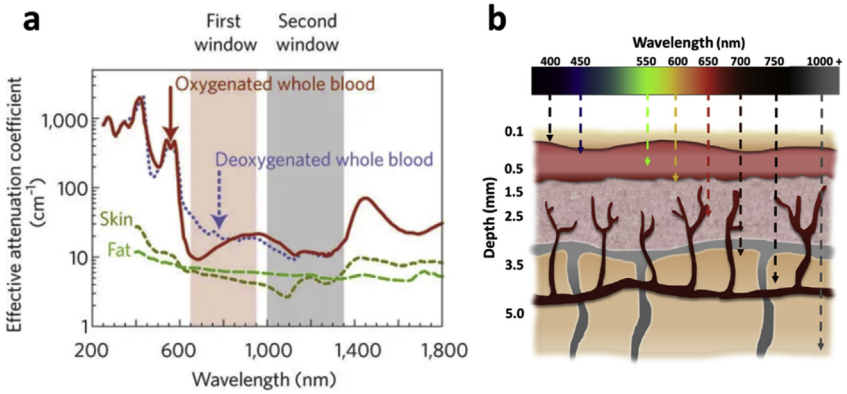


Fig. 2. (a) Effective attenuation coefficient vs. wavelength showing that for skin, fat, and oxygenated and deoxygenated blood, absorption and scattering is lowest in the NIR-I and NIR-II windows – reprinted by permission from Springer Nature: Nature Nanotechnology, [37], copyright (2009). (b) Schematic detailing penetration depth of light through biological tissue with respect to its wavelength.

into a measurable signal. Fluorescence biosensors form part of optical transducers whereby a fluorescence signal can be emitted, and the intensity quantified in correlation to biomarker concentration. To be used in a clinical setting, biosensors must meet numerous requirements, i.e. high accuracy, fast response times, repeatability, safety, and cost-effectiveness [46]. Methods used to synthesize these materials include top-down and bottom-up approaches, giving rise to ordered structures such as nanodisks, nanotriangles, and nanoholes and disordered nanostructures such as nanorods and nanoislands, which will be discussed in the following part of the article (Fig. 3).

Taking nanodisk fabrication as an example of a top-down synthesis method (Fig. 3a), monolayers of polystyrene spheres are first placed on a plasmonic surface. The uncovered surface is then etched out by reactive ion species, which, when the polystyrene template is removed, results in ordered nanodisk arrays. By reducing the size/increasing the spacing of the polystyrene spheres through O_2 plasma treatment, the resulting morphologies of the nanodisks can be tightly controlled. This templated lithography produces substrates which are highly reproducible and thus suitable for large-scale fabrication. The bottom-up method of substrate synthesis (Fig. 3b) usually involves synthesizing the nanostructures, such as nanorods, either directly onto the substrates or in solution and then casting them onto functionalized substrates. This can allow for a wider variety of substrate morphologies to be used, and although it is possible to create highly ordered substrates through this method, it is labor-intensive.

A limiting factor in the use of fluorescence biosensing for early detection, however, is its lack of sensitivity [9]. This is due to the fact that the intensity of the fluorescence signal being detected is dependent on the amount of disease biomarker present. Naturally, patients in the early stages of diseases such as cancer will present with very low biomarker concentrations in their body fluid, meaning that the fluorescence signal from the fluorophore-biomarker conjugates are very low in intensity, making reliable quantification difficult. When considering biosensing through biological medium (e.g. blood), there are poor signal-to-noise ratios which again limit their applicability. Therefore, to lower the detection limits of these biosensors, their sensitivity needs to be improved. By incorporating MEF into their design, the nanostructure-fluorophore coupled system enhances the signal, allowing detection even at lower biomarker concentrations (Fig. 4) [42]. Work discussed in this next section will focus on the design of MEF-biosensing platforms that operate within the NIR-I and NIR-II ranges of the electromagnetic spectrum.

Sun et al. [47] designed highly uniform and reproducible poly(methyl methacrylate) (PMMA)–coated Au@Ag nanorod arrays (Fig. 5a and b), which achieved fluorescence enhancement of up to 27 times of crystal violet. By creating more order to similar nanostructures, work carried out by Park et al. [48] showed nanoparticles-spiked pillar arrays (Fig. 5c and d) affording more than 270 times fluorescence enhancement using AlexaFluor® 647 as the fluorophore and more than 8.3×10^8 times SERS enhancement using the Raman-active methylene blue.

Pang et al. [49] investigated the fluorescence-enhancing capabilities of nanodisk arrays (Fig. 6a) on the commercially available NIR dye, AlexaFluor® 750. By modifying the structural characteristics of the nanodisk arrays (particle size and interparticle distance) while keeping the LSPR of the arrays centered around 750 nm, they were able to investigate the role of these structural characteristics on the magnitude of fluorescence enhancement achievable. All the nanodisk substrates exhibited significant fluorescence enhancement, with enhancement factors up to 235 times from the substrates with the largest particle size and smallest particle separation (~260 nm and 34 nm). Fluorescence lifetime measurements showed that, in the presence of the gold nanodisks, the radiative decay rates of the dye were significantly increased, reducing the lifetimes and increasing the quantum yield to above 90%.

Improving upon this nanostructure, Pang et al. [50] then developed a three-dimensional array consisting of nanodisks raised above nanoholes in a gold thin film (Fig. 6b), which, due to their synthesis *via* nanosphere lithography, exhibit uniform optical tunability relating to their disk diameter, pitch length, and thickness of gold (Fig. 7). Based on these parameters, the arrays' optical features can span in the NIR-I and NIR-II regions, enabling them to be spectrally coupled to multiple fluorophores for the development of multiplexed biosensors. In this investigation, the coupled effect of the array's LSPR and enhanced surface plasmon polaritons (SPPs) was used to enhance the fluorescence of the NIR dye, AlexaFluor® 790, by up to 400 times. Interestingly though, the computational electromagnetic modeling of these nanostructures indicates that

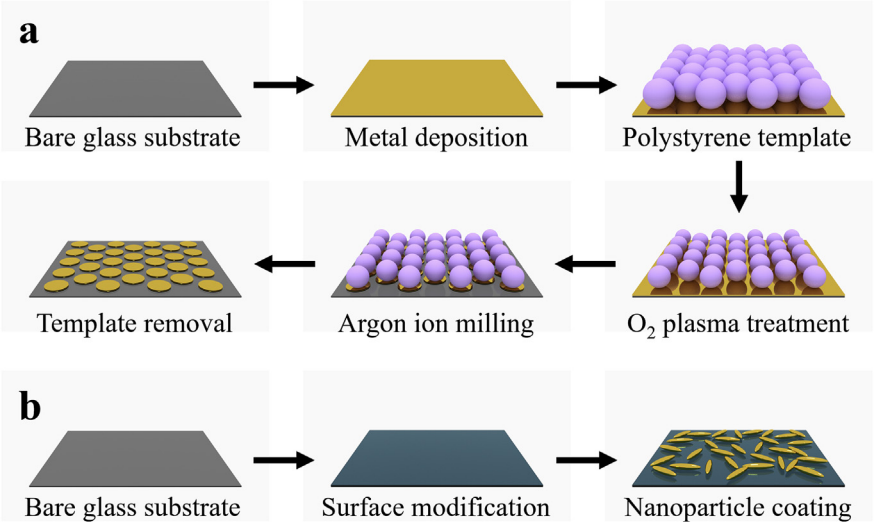


Fig. 3. Two schematic diagrams illustrating the methods of top-down (a) and bottom-up (b) substrate fabrication.

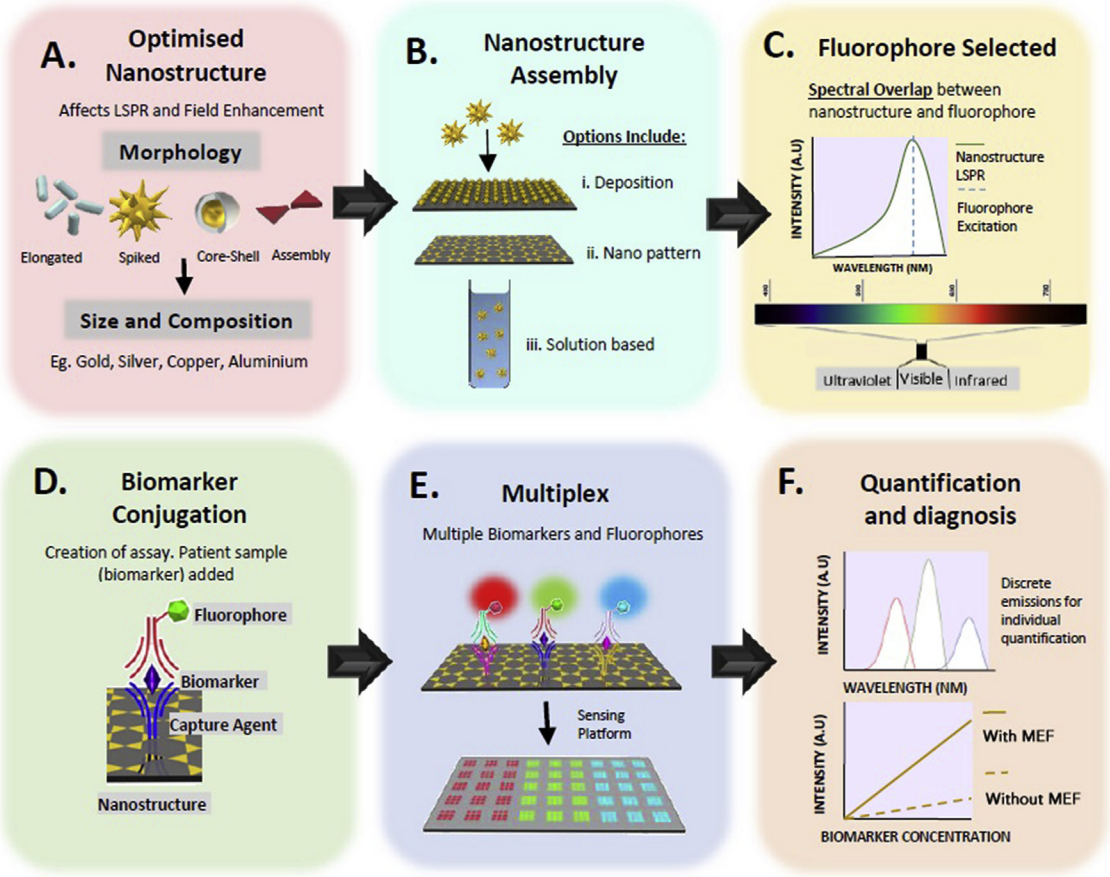


Fig. 4. (a–f) Fundamental steps for the design of an MEF-based biosensor. (a) Optimization of a nanostructure. Suitable electromagnetic field enhancements are required for specific disease biomarker detection. The morphology, materials, and size must be selected accordingly. (b) Platform assembly, nanopattern or solution preparation of the optimized nanostructure. (c) Choice of fluorophore and spectral region. For increased fluorescence intensity, an overlap between a fluorophore and metallic nanostructure optical properties must be present. (d) Disease-specific biomarkers identified. Capture agent immobilized on nanostructure. Patient sample (biomarker) added. Dye-conjugated system (e) move toward multiplexing, allowing for multiple biomarkers to be simultaneously analyzed. (f) Quantification and early diagnosis of disease with enhanced fluorescence intensity. Adapted with permission of Royal Society of Chemistry, from the study by Fothergill et al. [9], copyright (2018). MEF, metal-enhanced fluorescence; LSPR, localized surface plasmon resonance.

the excitation enhancement caused by the increased electric field should be on the level of three orders of magnitude, as opposed to the two orders of magnitude observed experimentally. Two possible reasons for this could be the increased disorder in the experimental vs. the computational model, as well as the gold film absorbing a portion of the fluorophore's emissions. As shown in computational work by Centeno et al. [55], emissions perpendicular to the surface of a plasmonic sphere will be enhanced, while others will be absorbed. In the case of this nanostructure, emissions which are normal to the edges of the nanodisks could be absorbed by the gold film of the nanohole array and *vice versa*. Further investigations are needed to optimize this structure for the highest possible fluorescence enhancement; however, this morphology is highly promising as a low-cost and reproducible (i.e. colloidal lithography) means of designing multiplexed NIR-I/NIR-II biosensors.

Nanotriangles are another nanostructure capable of significantly enhancing fluorescent dyes (Fig. 6). They are synthesized using similar techniques to nanodisks and form highly ordered hexagonal closely packed arrays [56]. Work by Xie et al. has extensively examined the fluorescence-enhancing effects of both silver [57] and gold [56] nanotriangles, but for the sake of this review, we will discuss their results of significant MEF in the NIR-II from a gold nanotriangle substrate with a quantum dot (QD) fluorophore, Ag_2S [58]. The reason for shifting to the NIR-II is the further reduced light scattering, absorption, and autofluorescence by biological material, enabling more sensitive detection and deeper tissue penetration. This is particularly important to enable the possibility of fluorescence diagnostics through blood.

In this investigation, two sizes of QD with emissions at 1100 nm and 1200 nm were immobilized onto gold nanotriangle arrays [58]. By tuning their interdistance spacing, the nanotriangles were fabricated to have LSPR peaks at 1200 nm and above. It was observed that significant fluorescence enhancement of 103 times was achieved for the 1200-nm-emitting QD, whereas 11.9 times enhancement was obtained for the 1100-nm-emitting QD. This has been attributed to the position of the fluorophore emission peaks relative to the LSPR of the nanotriangles. Previous work has shown that molecules emitting at shorter wavelengths than the LSPR experience more quenching, whereas molecules emitting at longer wavelengths experience stronger enhancement [56]. Finite-difference time-domain modeling has been used to calculate the absorption, scattering, and extinction efficiencies of gold and silver nanospheres, 80 nm in size. This showed that, while silver particles exhibited greater scattering efficiencies, the optical properties of gold particles were absorption-dominant [55]. As it has been shown that scattering efficiency relates to fluorescence enhancement, and absorption efficiency correlates to quenching [59], it is

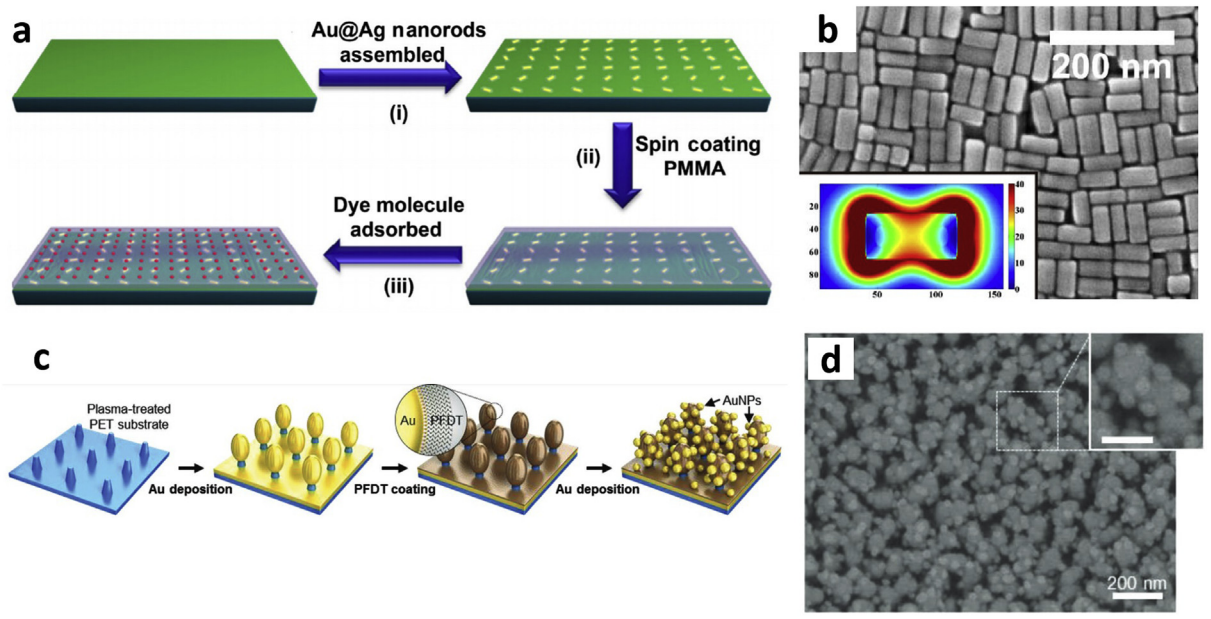


Fig. 5. (a–b) Au@Ag nanorod assemblies – reprinted by permission from Springer Nature: Nano Research, from the study by Sun et al. [47], copyright (2018). (a) Schematic of the synthesis method of Au@Ag nanorod assembly substrates. (b) Scanning electron image of Au@Ag nanorods; the inset shows the electric field intensity at the resonance peak of 614 nm. (c–d) Au-spiked pillar arrays – reproduced from the study by Park et al. [48] with permission from John Wiley and Sons: Advanced Functional Materials, copyright (2019). (c) Schematic of the fabrication procedure of Au-spiked pillar arrays. (d) Scanning electron image of Au-spiked nanopillars; the scale bar in the inset is 100 nm. PET, polyethylene terephthalate; PMMA, poly(methyl methacrylate); PFDT, perfluorodecanethiol.

expected that gold nanostructures will display some quenching at wavelengths less than their LSPR peak. The intense fluorescence enhancement achievable when the LSPR of the nanotriangle assay is matched to the corresponding Ag_2S QD emission peak; however, it shows the promise that this MEF platform has in dramatically improving the sensitivity of biosensing devices in the NIR-II region.

In addition to achieving great enhancement in the NIR-II using nanotriangular arrays (Fig. 6c), further work by Jawad et al. [51] has also utilized this nanostructure in the design of an ultrasensitive immunoassay for the detection of the pancreatic cancer biomarker CA 19-9, using the NIR-I dye, DyLight800. In this work, a sandwich protein microarray was incorporated onto a gold nanotriangle substrate (Fig. 8a). This substrate had been designed specifically to have its LSPR overlap with the fluorophore's spectral properties. Using this MEF system, they demonstrated its capability to accurately detect the CA 19-9 biomarker to a detection limit of

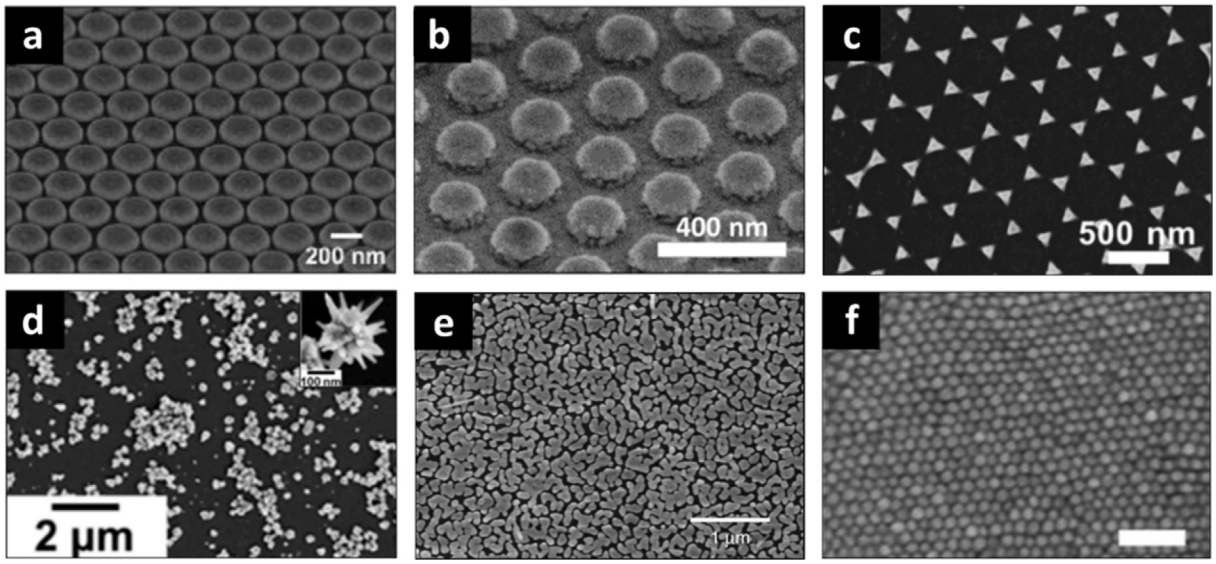


Fig. 6. (a–f) Scanning electron microscopy images of substrates for MEF (a) Au nanodisks – republished with permission of Royal Society of Chemistry, from Pang et al. [49] copyright (2013). (b) Au nanohole-disk array – reprinted with permission from Pang et al. [50], https://pubs.acs.org/doi/10.1021/acsami.9b08802. Copyright (2019) American Chemical Society (c) Au nanotriangles – reprinted from Nature Scientific Reports, https://doi.org/10.1038/s41598-017-14688-z, from Jawad et al. [51]. (d) Au nanostars – reprinted with permission from Theodorou et al. [52]. Copyright (2017), American Chemical Society. (e) Au nanoislands from a pGOLD™ slide – reprinted with permission from Springer Nature: Nature Medicine, from Zhang et al. [53], copyright (2014). (f) Top surface of a highly ordered Au nanorod supercrystal – reprinted with permission from Hamon et al. [54], https://pubs.acs.org/doi/abs/10.1021/acsphotonics.5b00369. Copyright (2015) American Chemical Society.

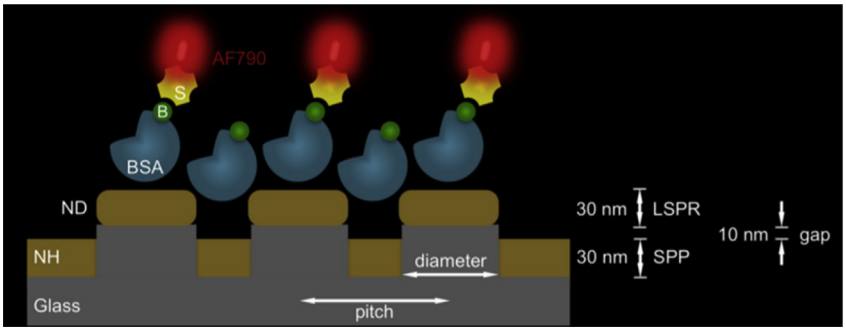


Fig. 7. Cross section of Au nanohole-nanodisk (NH-ND) array, functionalized with self-assembled monolayers of biotinated bovine serum albumin (bBSA), and streptavidin-bound AlexaFluor® 790 – reprinted with permission from Pang et al. [50], https://pubs.acs.org/doi/10.1021/acsami.9b08802. Copyright (2019) American Chemical Society.

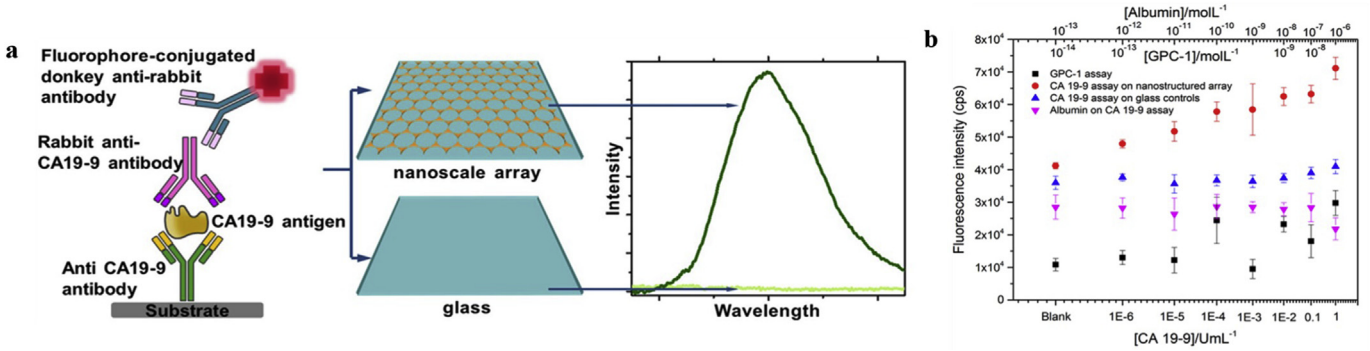


Fig. 8. NIR fluorescence enhancement immunoassay using nanotriangles for the quantification of the pancreatic cancer biomarker CA 19-9 shows far superior detection sensitivity relative to glass controls. Illustrated here are (a) the schematics for the CA 19-9 'sandwich' protein microarray, which, when performed on gold nanotriangle substrates, show fluorescence enhancement of up to two orders of magnitude compared with glass control substrates and (b) calibration curve for CA 19-9 quantification (red circles), showing biomarker detection at ultralow concentrations – reprinted from Nature Scientific Reports, https://doi.org/10.1038/s41598-017-14688-z, with permission from Jawad et al. [51]. NIR, near-infrared. (For interpretation of the references to colour in this figure legend, the reader is referred to the Web version of this article.)

7.7×10^{-7} U mL^{-1} (shown in Fig. 8), significantly lower than the lower limit of 35 U mL^{-1} currently used in the clinical setting [43]. Further work is ongoing to optimize this assay on different substrates, to further increase the sensitivity and to incorporate as part of a multiplexed assay to detect multiple markers associated with pancreatic cancer.

Au nanostars, consisting of a spherical core with several protruding branches, possess very strong LSPRs in the NIR-I/NIR-II region, with particularly enhanced (several orders of magnitude) electric field enhancements at the ends of their sharp tips and edges [60] and thus greatly concentrate the light surrounding the particle (Fig. 6d) [61]. They are highly promising MEF tools owing to the ease at which their optical properties can be modified across the NIR-I to NIR-II. In addition to this, their extinction spectra have been shown to be dominated by their photon scattering cross sections rather than absorption cross sections [62], which is key in generating far field radiation and thus enabling significant fluorescence enhancement. In work carried out by Theodorou et al. [52], using an Au nanostar substrate with an LSPR spanning from 700 to 1200 nm, fluorescence enhancements were achieved for fluorophores spanning from the NIR-I to the NIR-II. Over 190 times enhancement for AlexaFluor® 750, over 320 times enhancement for AlexaFluor® 790, and over 45 times enhancement for 1200-nm-emitting Ag_2S QDs were observed. These plasmonic Au nanostar substrates show great promise for the future development of ultrasensitive MEF biosensor platforms.

Extensive work on Au nanoisland films (Fig. 6e), known as plasmonic Au (pGOLD™) slides by Tabakman et al. [64], has shown its usefulness as a versatile substrate to greatly enhance fluorescence emission by NIR-I dyes over a broad wavelength range. Early research into this substrate showed its potential to, when incorporated into multiplexed protein microarrays, decrease the detection limits by three orders of magnitude down to the femtomolar scale (Fig. 9). This simple-to-fabricate substrate has since been used as a component in the ultrasensitive fluorescence-based detection of numerous analytes, such as lung cancer biomarkers [63], cardiovascular autoantibodies [65], diabetes biomarkers [53], toxoplasma [66], and Zika virus [67]. These assays have all demonstrated very low limits of detection, and as such, very little biological samples (as little as 1 μL of serum or whole blood) [68] are needed to produce a clear result. This plasmonic nanostructure, with its scalable synthesis, reproducibility, and high sensitivity could be the next step in high-throughput screening of a whole range of diseases, including various cancers.

5. Fluorescence imaging

In medical textbooks, to aid the readers' understanding of the anatomy of the human body, different tissues are color-coded (e.g. nerves in yellow, veins in blue). However, in surgery under white light – as is the case in the operating room – the internal tissues of a patient are substantially harder to differentiate, with colors ranging from shades of pinks (nerves and muscle) to reds (blood vessels) to deep reds (organs) [69]. As surgery is still the primary treatment for many types of cancers, one of the greatest surgical challenges today lies in determining exactly where healthy tissue

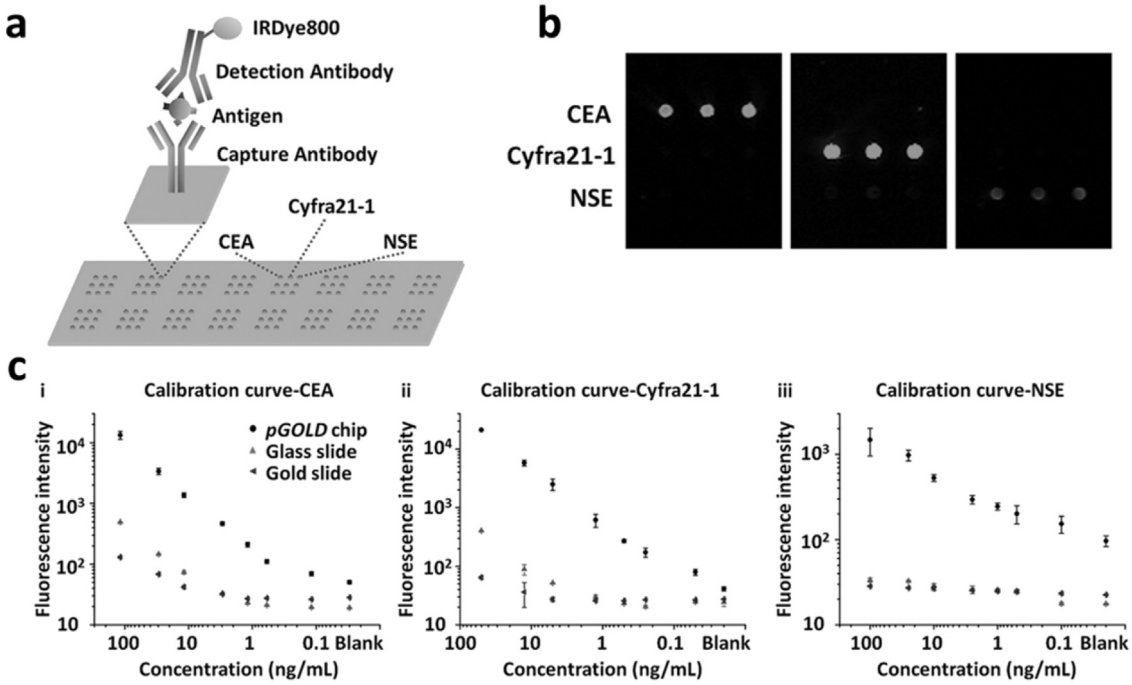


Fig. 9. (a) Schematic of the triple lung cancer biomarker (CEA, Cyfra21-1, and NSE) detection on a pGOLD™ slide. (b) Fluorescence images showing only one row of brightly fluorescing spots, produced upon incubating a multiplexed antibody chip in a solution containing a mixture of the three antigens, followed by incubation with only one of the corresponding detection antibodies. (c) Calibration curves comparing the detection limits and dynamic ranges of the three lung cancer biomarkers on pGOLD™ chips, glass, and Au slides – reproduced from the study by Liu et al. [63] with permission from John Wiley and Sons: Advanced Functional Materials, copyright (2016).

ends and cancerous tissue begins [20]. Overcutting tumors can lead to the unnecessary removal of healthy tissue, leading to potentially drastic results, while undercutting leaves cancer cells behind, resulting in tumor recurrence over time. Multiple studies have shown that positive margins (presence of tumor cells at the edge of removed tissue) are closely linked with increased local recurrence and indicate a poor survival rate in most cancers, including breast cancer [70], colorectal cancer [71], prostate cancer [72], and non-small-cell lung cancer [73].

As a result of this, to facilitate the operating surgeon in achieving the best outcome for the resection surgery, a series of preoperatively taken scans and images are used. These computed tomography (CT), magnetic resonance imaging (MRI), and/or positron emission tomography (PET) scans allow the surgeon to estimate the amount of tissue to be removed [74]. These scans are limited to the detection of tumors which have reached a certain threshold in size, i.e. several millimeters or approximately 10 million cells [20], meaning that many tumors remain undetected. Although substantial advances have been made in these imaging techniques in recent years, allowing them to produce comprehensive images which can greatly aid surgeons, they are unfit to be used in a real-time surgical procedure as they are plagued by a number of limitations: use of ionizing radiation, large machinery requirement, time-consuming image construction, high cost, and need for a specialist operator [75].

In comparison with these bioimaging modalities, fluorescence imaging has a number of distinct advantages, not least the fact that the equipment necessary is relatively low cost and portable, making it possible to be incorporated as a real-time imaging tool during operation [76]. It is a much safer alternative to CT and MRI, i.e. it uses non-ionizing radiation and has far superior resolving power (~100 μm) [77], making it possible to clearly define tumor boundaries and improve the rate of successful resection. By using highly specific fluorescent probes, it is possible to 'light up' the tissues of interest, be they cancerous tissues to be removed or vital nerves to be preserved in surgery [78].

Similarly to the biosensing advances discussed in this review, the focus of this section is on the design of ultrabright probes that both absorb and emit in the NIR to improve image resolution and also to increase the tissue penetration depth, giving surgeons a more comprehensive view of the site of surgery. There are two methods by which these fluorescent probes can target cancerous cells, thereby enabling sensitive and accurate imaging. These methods are passive targeting and active targeting [79,80]. Passive targeting relies on the enhanced permeability and retention of cancer cells and thus is dependent on the size of the particle, with particles between 30 and 200 nm showing good cell uptake efficiencies [81]. In active targeting, nanoprobes are conjugated to ligands such as antibodies and RNA, which selectively attach to antigens or receptors either on the surface or within the cancer cells [82]. It is not a design requirement that fluorescent nanoprobes be capable of being internalized by cancer cells but that they can attach to the cells, either internally or on their surface. As all the nanoprobes discussed here rely on active targeting for selective imaging, only their efficacy as fluorescence enhancers will be discussed.

Currently, many designs of materials enabling fluorescence enhancement in the NIR-I/II regions have been reported; however, these have predominantly focused on gold or silver nanostructured surfaces or particles immobilized on solid substrates. To date, few reports have been published regarding NIR fluorescence enhancement using colloidal nanoparticles, and of those reported, there are still a number of issues limiting their further development for widespread application [20,83].

As previously discussed, the magnitude of fluorescence enhancement is highly dependent on a number of factors, one of which being the spectral overlap between the LSPR of the metal nanoparticle and the excitation and emission wavelengths of the

fluorophore [84]. To achieve this spectral overlap, it is necessary to be able to tune the LSPR of the metal nanoparticle to match the spectral properties of the dye. Theodorou et al. [85] have investigated the design of imaging probes comprised of gold nanostars conjugated to either a NIR-I dye (DyLight800 or IRDye 800 CW) or a NIR-II dye (Ag_2S QDs) (Fig. 10). Substrate work based on this design showed the great promise nanostars have for greatly enhancing the fluorescence of long-wavelength dyes, owing to their broad LSPRs in the NIR, their high-scattering cross sections, and their sharp, branched structure (Fig. 10b and c) creating intense electromagnetic 'hot spots' at their spike tips [52]. In their recent work, two types of nanostars – ~50 nm and ~250 nm – with controlled LSPRs in the NIR-I and NIR-II regions were used. Significant single-particle fluorescence enhancement of up to 30-fold was obtained for the NIR-I dyes, while up to 4 times enhancement was achieved for the NIR-II QDs (Fig. 10d–f). The enhancement factors obtained using the smaller nanostars were slightly lower than those from the larger nanostars – 20-fold vs. 30-fold – however, owing to their much smaller size, they show more potential for *in vivo* imaging applications.

Ayala-Orozco et al. [86] reported fluorescence enhancements of the NIR-I dyes Cy7 and IR800 by ~16 times, using an $Au@SiO_2@Au$ multiple shelled structure, dubbed a nanomatryoshka (Fig. 11). The plasmon resonances of the Au core and Au shell strongly interact with each other and create hybridized modes in the NIR. When the dyes are placed in between this Au core and shell, they experience intense near-field enhancement of the excitation light, leading to substantial fluorescence enhancement.

Xu et al. [87] developed a novel 'turn-on' MEF nanoprobe for *in situ* visualization of telomerase activity in live cells. This probe consisted of Au nanobipyramids functionalized with Cy5.5-labeled DNA sequences, which achieved fluorescence enhancement of over 10 times and enabled the distinction between healthy and cancerous cells, which exhibit low and high telomerase activity, respectively.

Work by Sun et al. [88] on MEF cell imaging involved the detection of micro-RNA biomarker expression levels in live cells. This was done using an Au nanocross/Au nanorod conjugate, functionalized with the dye Cy5, which would turn on upon attachment to micro-RNA-21 (Fig. 12). An enhancement factor of over 10 times was obtained, which allowed the ultrasensitive detection of micro-RNA biomarkers in living cells, with a detection limit of 0.03 fM. Luo et al. [89] designed a turn-on fluorescent nanorod conjugate for intercellular and extracellular H_2S detection, with 5 times fluorescence enhancement of the porphyrin dye used. Sensitive detection of H_2S in solution as low as 17 nM, as well as *in situ* H_2S imaging in living cells, was achieved using this plasmonic nanoprobe.

Another on-off fluorescence nanoprobe design by Yu et al. [90] allowed detection limits orders of magnitude lower than what is currently available (on a micromolar level) for the biomolecule adenosine triphosphate (ATP). Au nanorods were functionalized with a polyethylene glycol (PEG)–modified DNA sequence, upon which IRDye 800 CW was attached. In the absence of ATP, the DNA sequence would self-hybridize and fold in on itself, bringing the dye in such close proximity to the gold nanorod that quenching would occur. However, in the presence of ATP, the DNA self-hybridization would be interrupted, thus moving the fluorophore further from the Au nanorod surface and into a position where maximum fluorescence enhancement could occur. This resulted in fluorescence enhancement of the IRDye CW by up to 235 times and a resulting detection limit of ~0.6 nM. The sensitive intracellular

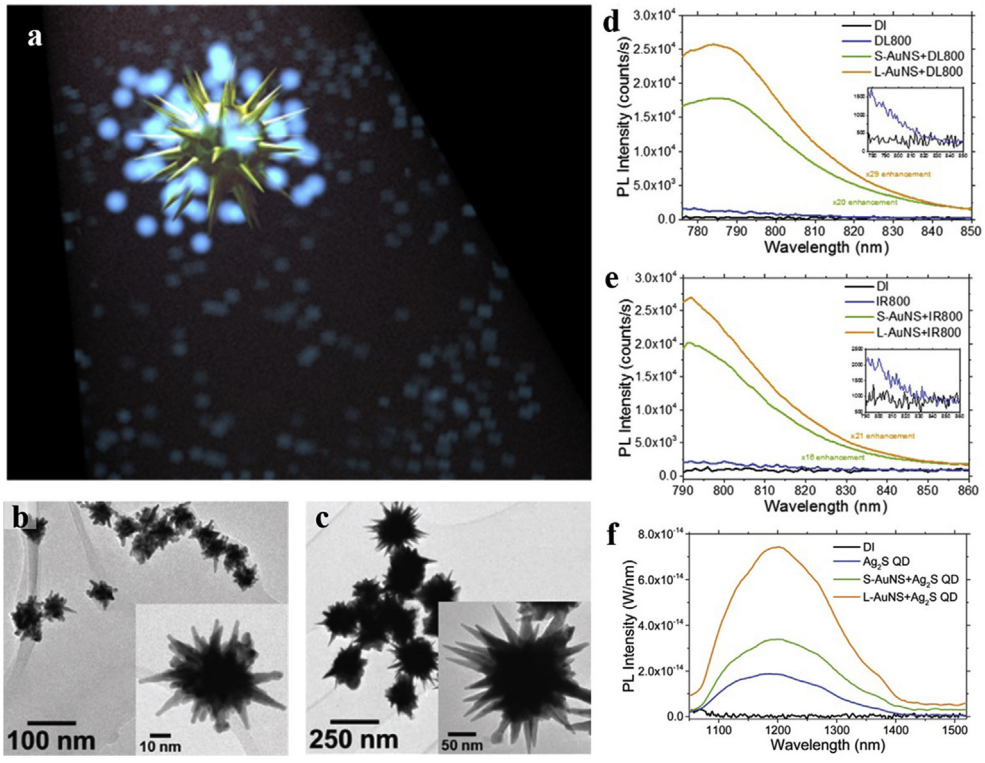


Fig. 10. (a) Schematic showing the ultrabright fluorescence obtained from the nanostar MEF probes in comparison with free fluorophores in solution; (b–c) schematic showing transmission electron microscopy images of the two different nanostar morphologies investigated; (d–f) graphs showing photoluminescence emission spectra of (d) DyLight800, (e) IR800, and (f) Ag_2S quantum dots conjugated to small and large nanostars, measured against equivalent amounts of free fluorophores, with deionized water (DI) used for background correction – republished with permission from Royal Society of Chemistry, from Theodorou et al. [85], copyright (2018). MEF, metal-enhanced fluorescence; PL, photoluminescence.

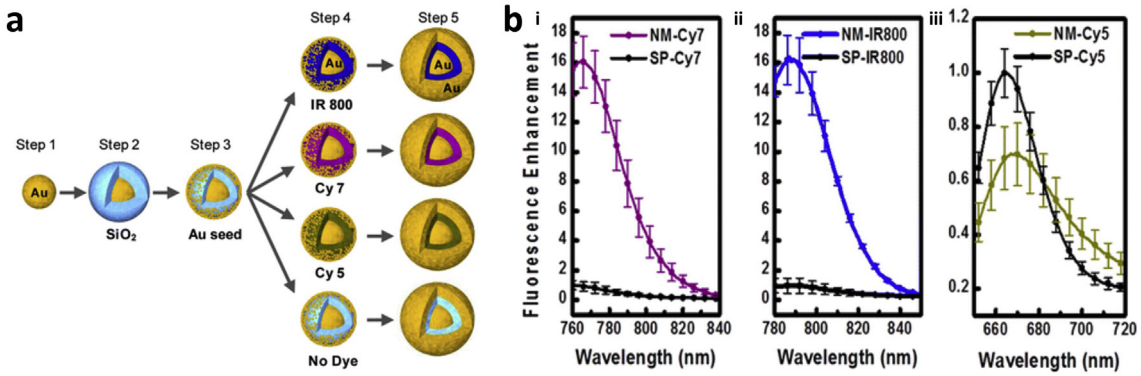


Fig. 11. (a) Schematic demonstrating the particle morphology over the course of the synthesis, from an unfunctionalized Au sphere, to a coating in APTES-doped silica, to an Au@SiO_2 core-shell particle decorated with small Au colloids, to a seeded precursor nanoparticle doped with fluorescent dyes and finally an Au nanomatryoshka with fluorescent dye in the silica spacer. (b) Photoluminescence emission spectra of (i) Cy7, (ii) IR800, and (iii) Cy5 dyes confined inside the nanomatryoshka (NM), compared with the dyes conjugated to the corresponding seeded precursors (SPs). Reprinted with permission from Ayala-Orazco et al. [86], https://pubs.acs.org/doi/10.1021/nl501027j. Copyright (2014) American Chemical Society.

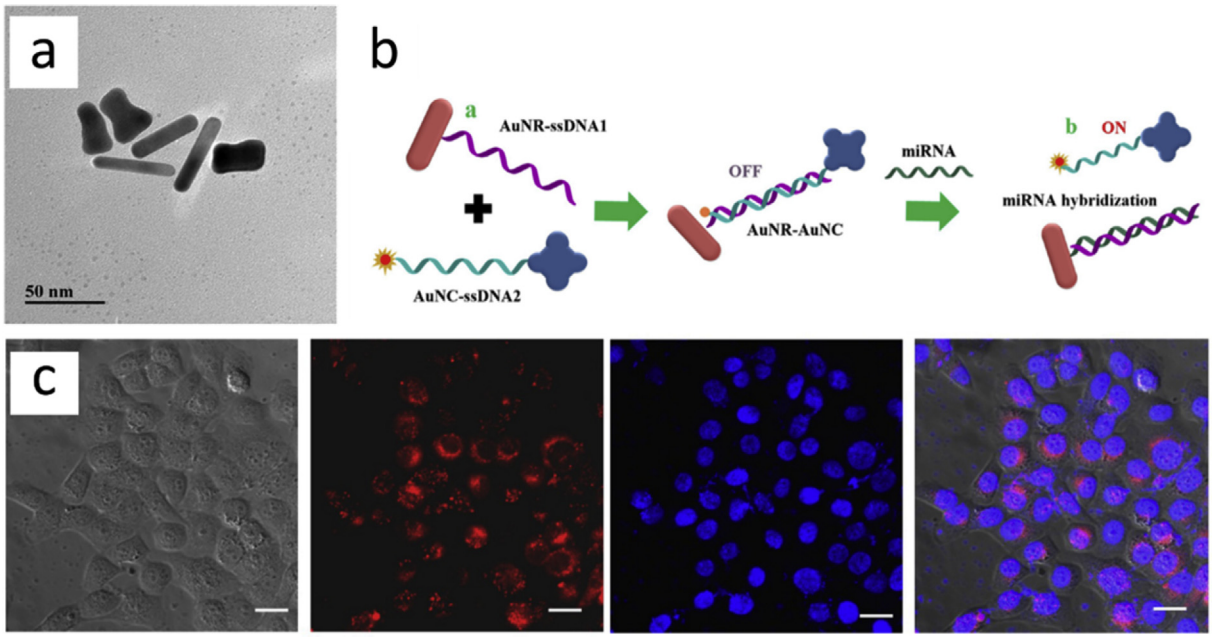


Fig. 12. (a) Transmission electron microscopy image of the Au nanocross decorated with nanorods. (b) Schematic of the off/on fluorescent switching system for the detection of miRNAs in living cancer cells. (c) Confocal fluorescence images of Au nanorod/nanocrosses in HepG2 cells, showing the presence of miRNA-21. Left to right: bright field, red field, blue field, and merged images. Scale bar: 20 μm. Adapted with permission from Sun et al. [88]. Copyright (2018) American Chemical Society. (For interpretation of the references to color in this figure legend, the reader is referred to the Web version of this article.)

detection of ATP levels could help determine cell health and thus provide vital information for disease diagnosis [91].

Significant fluorescence enhancement using Au nanocubes was obtained by Xu et al. [92]. In this work, nanocubes of ~45 nm were conjugated to sulfonated aluminum phthalocyanine, a clinically approved photosensitizer for photodynamic therapy of cancer, which fluoresces at 680 nm. By adjusting the ratio of fluorophore to plasmonic particle, enhancement factors of over 60 times were achieved, with 5 μM of fluorophore to 50 pM of Au nanocubes producing an enhancement of 150 times in water. Incorporating these particles into fluorescence imaging of HeLa cells afforded a 300 times fluorescence enhancement. Not only does this nanoprobe design show promise as a cancer-imaging agent but also as a theranostic agent, owing to the photosensitizing properties of sulfonated aluminum phthalocyanine.

In recent research by Theodorou et al. [93], gold nanostar substrates similar to ones discussed in Section 2 were used to replace standard glass slides as mounts for cell imaging. In this work, two nanostar substrates were prepared *via* the bottom-up approach, where in-house synthesized gold nanostars of either small (~50 nm) or large (215 nm) sizes were fixed to a glass substrate. Then, cervical cancer HeLa cells — which overexpress folate receptor alpha (FRα) — were labeled with the FRα polyclonal antibody and subsequently counterstained with AlexaFluor® 680. These stained cells were then fixed to both the gold nanostar substrates and to bare glass, and confocal microscopy was performed on the samples (Fig. 13). What was found was that the fluorescence signal of the AF680 from the surface of the HeLa cells was significantly higher on the small and large nanostar arrays (approximately 9 and 19 times, respectively) than from the cells on the plain glass. This

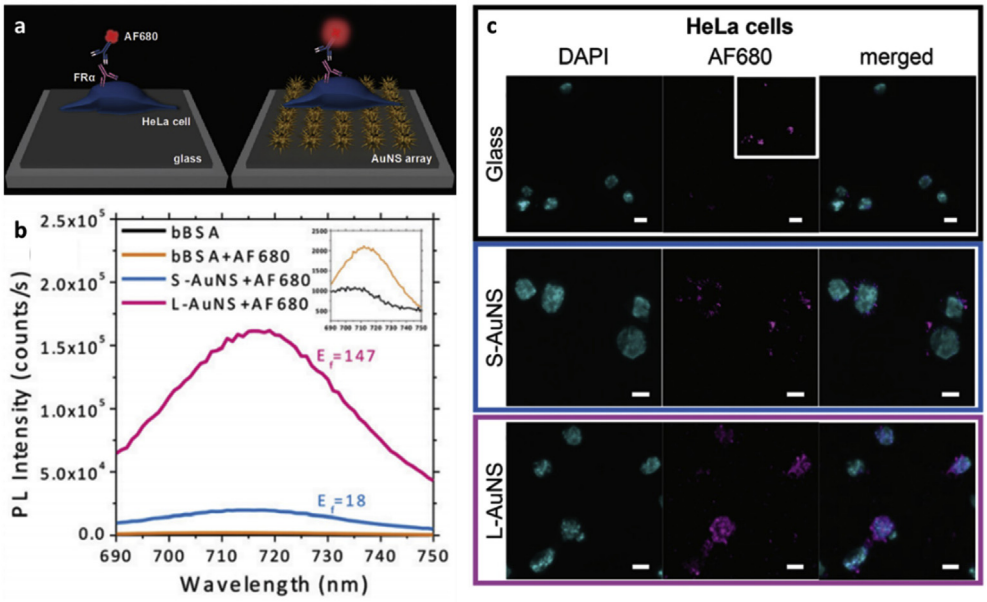


Fig. 13. (a) Schematic illustration of the fluorescence-enhanced cellular assay using gold nanostars. (b) Photoluminescence (PL) emission spectra of monolayers of AlexaFluor® 680 formed on biotinated bovine serum albumin (bBSA)–coated glass slides and on small and large nanostar arrays. (c) Images of DAPI (4′6-diamidino-2-phenylindole) (cyan)-labeled and AlexaFluor® 680 (magenta)–labeled HeLa cells, as well as their merged signals on glass, small and large nanostar substrates. Adapted with permission of Royal Society of Chemistry, from Theodorou et al. [93], copyright (2019). (For interpretation of the references to colour in this figure legend, the reader is referred to the Web version of this article.)

indicates that, by modifying the strength of the electric field around the nanostars through changing their morphology, cellular imaging with increased fluorescence contrast can be achieved. Moreover, owing to the strong dependence of the nanostar LSPR on the shape and size of the particles, substrates can be developed with field enhancements over a range of wavelengths, allowing a multitude of cell stain intensities to be improved upon for novel multicolor and multiplexed imaging platforms.

As previously mentioned in section 4, pGOLD™ chips (Fig. 6e) have the capability of greatly enhancing the fluorescence of NIR-I dyes and, as such, have been investigated as highly sensitive biosensing materials [53,66–68]. Similar to Au nanostar substrates, these Au nanoisland substrates have also shown great promise for cell imaging [94]. Work by Koh et al. [94] has shown ~3 times fluorescence enhancement for the visible stains Cy3 and Cy5 and roughly 30 times enhancement for the NIR-I stains IRDye 680 and IRDye 800, enabling multicolor cell imaging and protein detection with high signal-to-background ratios over a wide range of 500–700 nm. This work and work on the Au nanostar substrates [52] highlight the potential of plasmonic chips to enable high-performance multiplexed biological imaging with both research and diagnostic applications.

6. Particle toxicity

As described earlier, Au nanostructures show promise to be used not only in fluorescence-based biosensors for disease diagnosis but also for fluorescence imaging in the biologically transparent NIR windows. Nonetheless, it is necessary to also consider the potential side-effects of using these plasmonic particles in patients. Numerous studies have investigated the cytotoxicity [95], biodistribution [96], and retention time [97] of Au nanoparticles, as well as the effect particle size and shape had on these parameters. However, many published articles appear to challenge each other. Surface charge, for example, is regularly reported as being a key factor in the toxicity of Au nanoparticles, with positive particles exhibiting more toxic effects than negative or neutral particles [98], yet elsewhere it has been found that neither negative nor positive Au particles possess toxicity to cells [99,100]. The correlation between particle size and toxicity is another instance in which there are conflicting results. Where one study quotes that larger, 50-nm Au particles show higher toxicity to breast cancer cells than smaller, 13-nm particles [101], another contradicts this, showing that it was the smaller, 8-nm Au particles that were more cytotoxic to hepatic cells than larger, 37-nm particles [102]. These inconsistencies are due to the unique physicochemical nature of nanoparticles, and as such, there is no single standardized assay which can be applied to test the toxicity effect of all nanoparticles [20].

As of yet, there are no clinical trials concerning Au nanoparticles as fluorescence imaging enhancers in the NIR region; however, there are numerous ongoing clinical trials involving Au nanoparticles as a means of treating cancer either by means of drug delivery or through photothermal therapy in the NIR window. For example, the Nanospectra project, Aurolase®, is currently in clinical trials for the laser-assisted photothermal ablation of prostate cancer cells. This Au nanoparticle consists of a silica-Au nanoshell coated in PEG and exhibits an LSPR in the NIR-I [103]. The latest published data on this nanostructure show that 12 months after Aurolase® treatment, 89% of patients presented with no cancer within the ablation zones [104].

Although this Au nanostructure is being used as a photothermal treatment and not a fluorescence imaging agent, the positive results of this trial could pave the way for future trials involving Au nanoparticles as cancer-imaging probes. In particular, with regards to surgical guided imaging, the Au-based probes could be introduced intravenously and allowed to accumulate predominantly on or in the cancerous tissue. Then the majority of the particles could be removed along with the excised tumors, meaning that the only trace amounts of the particles would remain in the body (in the liver and spleen, for example, [105,106]), potentially having minimum potency. Interestingly, Li et al. [107] recently demonstrated the high clearance rates (over 90% excreted 72 h after injection) of liposome-coated, lanthanide-based fluorescent particles. These particles, although above 70 nm in size, were cleared *via* the

hepatobiliary route, clearly demonstrating the potential liposomes have in addressing potential toxicity and clearance issues many nanoparticle probes, including Au-based, have. Nevertheless, it is evident that further studies and investigation into both the long- and short-term toxicity is required.

7. Conclusion

MEF is an optical process that produces amplified fluorescence, induced by metallic nanostructures near fluorophores, under specific conditions. This light amplification may be exploited to considerably increase detection sensitivity, therefore improving the performance of fluorescence-based sensing technologies. Meanwhile, the presence of metallic nanostructures could not only enhance fluorescence but also stabilize fluorophores against photobleaching, further enhancing their applications in bioimaging. MEF provides a paradigm shift in the biomedical engineering field. From the work carried out by the groups discussed in this review, it is evident that the applicability of MEF technology has great potential to impact ultrasensitive biosensing and super-resolution bioimaging toward the NIR-I/NIR-II window. Indeed, MEF has a bright future in biomedical research, diagnosis, and treatment.

Declaration of competing interest

The authors declare that they have no known competing financial interests or personal relationships that could have appeared to influence the work reported in this paper.

Acknowledgments

The authors acknowledge the EPSRC Centre for Doctoral Training in Advanced Characterisation of Materials (EP/L015277/1), the EPSRC DTP training grant (EP/N509486/1), and the British Council Newton Grant (No. 216239013) for financial support.

References

[1] S. Eustis, et al., Why gold nanoparticles are more precious than pretty gold: noble metal surface plasmon resonance and its enhancement of the radiative and nonradiative properties of nanocrystals of different shapes, Chem. Soc. Rev. 35 (3) (2006) 209–217, https://doi.org/10.1039/B514191E.
[2] Y. Kou, J. Wang, C. Chen, Research progresses for tumor theranostics based on gold nanomaterials, Chin. J. Clin. Oncol. 41 (1) (15-Jan-2014) 51–55, https://doi.org/10.3969/j.issn.1000-8179.20131768.
[3] P. Pedrosa, R. Vinhas, A. Fernandes, P. V Baptista, Gold nanotheranostics: proof-of-concept or clinical tool? Nanomaterials (Basel, Switzerland) 5 (4) (Nov. 2015) 1853–1879, https://doi.org/10.3390/nano5041853.
[4] D. Darvill, A. Centeno, F. Xie, Plasmonic fluorescence enhancement by metal nanostructures: shaping the future of bionanotechnology, Phys. Chem. Chem. Phys. 15 (38) (Sep. 2013) 15709, https://doi.org/10.1039/c3cp50415h.
[5] S. Cui, S. Zhang, S. Yue, Raman spectroscopy and imaging for cancer diagnosis, J. Helathcare Eng. 2018 (2018), https://doi.org/10.1155/2018/8619342. Hindawi Limited.
[6] M.I. Khot, H. Andrew, H.S. Svavarsdottir, G. Armstrong, A.J. Quyn, D.G. Jayne, "A review on the scope of photothermal therapy–based nanomedicines in preclinical models of colorectal cancer, Clin. Colorectal Canc. 18 (2) (01-Jun-2019) e200–e209, https://doi.org/10.1016/j.clcc.2019.02.001. Elsevier Inc.
[7] M. Tampa, et al., Photodynamic therapy: a hot topic in dermato-oncology (Review), Oncol. Lett. 17 (5) (May 2019) 4085–4093, https://doi.org/10.3892/ol.2019.9939.
[8] J.-E. Park, M. Kim, J.-H. Hwang, J.-M. Nam, Golden opportunities: plasmonic gold nanostructures for biomedical applications based on the second near-infrared window, Small Methods 1 (3) (Mar. 2017) 1600032, https://doi.org/10.1002/smtd.201600032.
[9] S.M. Fothergill, C. Joyce, F. Xie, Metal enhanced fluorescence biosensing: from ultra-violet towards second near-infrared window, Nanoscale 10 (45) (Nov. 2018) 20914–20929, https://doi.org/10.1039/C8NR06156D.
[10] W. Deng, E.M. Goldys, Plasmonic approach to enhanced fluorescence for applications in biotechnology and the life sciences, Langmuir 28 (27) (Jul. 2012) 10152–10163, https://doi.org/10.1021/la300332x.
[11] A.S. Baburin, A.M. Merzlikin, A.V. Baryshev, I.A. Ryzhikov, Y.V. Panfilov, I.A. Rodionov, Silver-based plasmonics: golden material platform and application challenges [Invited], Opt. Mater. Express 9 (2) (Feb. 2019) 611, https://doi.org/10.1364/ome.9.000611.
[12] F. Parveen, B. Sannakki, M.V. Mandke, H.M. Pathan, Copper nanoparticles: synthesis methods and its light harvesting performance, Sol. Energy Mater. Sol. Cell. vol. 144 (01-Jan-2016) 371–382, https://doi.org/10.1016/j.solmat.2015.08.033. Elsevier B.V.
[13] M. Jeyaraj, S. Gurunathan, M. Qasim, M.H. Kang, J.H. Kim, A comprehensive review on the synthesis, characterization, and biomedical application of platinum nanoparticles, Nanomaterials 9 (12) (01-Dec-2019), https://doi.org/10.3390/nano9121719. MDPI AG.
[14] U. Guler, V.M. Shalaev, A. Boltasseva, Nanoparticle plasmonics: going practical with transition metal nitrides, Mater. Today 18 (4) (01-May-2015) 227–237, https://doi.org/10.1016/j.mattod.2014.10.039. Elsevier.
[15] Y. Liu, M. Liu, M.T. Swihart, Plasmonic copper sulfide-based materials: a brief introduction to their synthesis, doping, alloying, and applications, J. Phys. Chem. C 121 (25) (Jun. 2017) 13435–13447, https://doi.org/10.1021/acs.jpcc.7b00894.
[16] A. Kumar, S. Kim, J.M. Nam, Plasmonically engineered nanoprobes for biomedical applications, J. Am. Chem. Soc. 138 (44) (09-Nov-2016) 14509–14525, https://doi.org/10.1021/jacs.6b09451. American Chemical Society.
[17] E. Petryayeva, U.J. Krull, "Localized surface plasmon resonance: nanostructures, bioassays and biosensing—a review, Anal. Chim. Acta 706 (1) (Nov. 2011) 8–24, https://doi.org/10.1016/j.aca.2011.08.020.
[18] M. Grzelczak, J. Pérez-Juste, P. Mulvaney, L.M. Liz-Marzán, Shape control in gold nanoparticle synthesis, Chem. Soc. Rev. 37 (9) (15-Aug-2008) 1783–1791, https://doi.org/10.1039/b711490g. The Royal Society of Chemistry.
[19] S. Zeng, K.T. Yong, I. Roy, X.Q. Dinh, X. Yu, F. Luan, A review on functionalized gold nanoparticles for biosensing applications, Plasmonics 6 (3) (Sep. 2011) 491–506, https://doi.org/10.1007/s11468-011-9228-1.
[20] P. Singh, S. Pandit, V.R.S.S. Mokkapati, A. Garg, V. Ravikumar, I. Mijakovic, Gold nanoparticles in diagnostics and therapeutics for human cancer, Int. J. Mol. Sci. 19 (7) (06-Jul-2018), https://doi.org/10.3390/ijms19071979. MDPI AG.
[21] C.D. Geddes, J.R. Lakowicz, Editorial Metal-Enhanced Fluorescence concentrating the local field and subsequently increasing nearby metal can increase the intrinsic radiative decay, J. Fluoresc. 12 (2) (2002).
[22] N. Gandra, et al., Probing distance-dependent plasmon-enhanced near-infrared fluorescence using polyelectrolyte multilayers as dielectric spacers, Angew. Chem. Int. Ed. 53 (3) (Jan. 2014) 866–870, https://doi.org/10.1002/anie.201308516.
[23] L. Zhu, M. Gao, C.K.N. Peh, G.W. Ho, Solar-driven photothermal nanostructured materials designs and prerequisites for evaporation and catalysis applications, Mater. Horizons 5 (3) (May 2018) 323–343, https://doi.org/10.1039/C7MH01064H.
[24] G. Hong, A.L. Antaris, H. Dai, Near-infrared fluorophores for biomedical imaging, Nature Biomed. Eng. 1 (1) (Jan. 2017) 10, https://doi.org/10.1038/s41551-016-0010.
[25] Y. Sun, et al., Novel bright-emission small-molecule NIR-II fluorophores for in vivo tumor imaging and image-guided surgery, Chem. Sci. 8 (5) (May 2017) 3489–3493, https://doi.org/10.1039/c7sc00251c.
[26] A.L. Antaris, et al., A small-molecule dye for NIR-II imaging, Nat. Mater. 15 (2) (Nov. 2015) 235–242, https://doi.org/10.1038/nmat4476.
[27] B. Li, L. Lu, M. Zhao, Z. Lei, F. Zhang, An efficient 1064 nm NIR-II excitation fluorescent molecular dye for deep-tissue high-resolution dynamic bioimaging, Angew. Chem. Int. Ed. 57 (25) (Jun. 2018) 7483–7487, https://doi.org/10.1002/anie.201801226.
[28] X. Yi, et al., IR-780 dye for near-infrared fluorescence imaging in prostate cancer, Med. Sci. Mon. Int. Med. J. Exp. Clin. Res. 21 (Feb. 2015) 511–517, https://doi.org/10.12659/MSM.892437.
[29] A.L. Antaris, et al., A high quantum yield molecule-protein complex fluorophore for near-infrared II imaging, Nat. Commun. 8 (May 2017) 15269, https://doi.org/10.1038/ncomms15269.
[30] R. Tang, J. Xue, B. Xu, D. Shen, G.P. Sudlow, S. Achilefu, Tunable ultrasmall visible-to-extended near-infrared emitting silver sulfide quantum dots for integrin-targeted cancer imaging, ACS Nano 9 (1) (Jan. 2015) 220–230, https://doi.org/10.1021/nn5071183.
[31] A.R. Young, Chromophores in human skin, Phys. Med. Biol. 42 (5) (May 1997) 789–802, https://doi.org/10.1088/0031-9155/42/5/004.
[32] J.P. Martin, N.R. Fetto, M.J. Tucker, Comparison of biological chromophores: photophysical properties of cyanophenylalanine derivatives, Phys. Chem. Chem. Phys. 18 (30) (2016) 20750–20757, https://doi.org/10.1039/c6cp04154j.
[33] S.L. Jacques, Optical properties of biological tissues: a review, Phys. Med. Biol. 58 (11) (07-Jun-2013), https://doi.org/10.1088/0031-9155/58/11/R37.
[34] A.N. Bashkatov, E.A. Genina, V.V. Tuchin, Optical properties of skin, subcutaneous, and muscle tissues: a review, J. Innovat. Opt. Health Sci. 4 (1) (Jan. 2011) 9–38, https://doi.org/10.1142/S1793545811001319.
[35] S. Diao, et al., Biological imaging without autofluorescence in the second near-infrared region, Nano Res. 8 (9) (Sep. 2015) 3027–3034, https://doi.org/10.1007/s12274-015-0808-9.
[36] J. V Frangioni, In vivo near-infrared fluorescence imaging, Curr. Opin. Chem. Biol. 7 (5) (Oct. 2003) 626–634, https://doi.org/10.1016/J.CBPA.2003.08.007.
[37] A.M. Smith, M.C. Mancini, S. Nie, Bioimaging: second window for in vivo imaging, Nat. Nanotechnol. 4 (2009) 710–711, https://doi.org/10.1038/nnano.2009.326.

[38] G. Hong, et al., Multifunctional in vivo vascular imaging using near-infrared II fluorescence, Nat. Med. 18 (12) (Dec. 2012) 1841–1846, https://doi.org/10.1038/nm.2995.

[39] G. Hong, et al., "Near-Infrared II fluorescence for imaging hindlimb vessel regeneration with dynamic tissue perfusion measurement," *circ*, Cardiovasc. Imag. 7 (3) (May 2014) 517–525, https://doi.org/10.1161/CIRCIMAGING.113.000305.

[40] R.L. Siegel, K.D. Miller, A. Jemal, Cancer statistics, CA – Cancer J. Clin. 67 (1) (Jan. 2017) 7–30, https://doi.org/10.3322/caac.21387.

[41] J.N. Anker, W.P. Hall, O. Lyandres, N.C. Shah, J. Zhao, R.P. Van Duyne, Biosensing with plasmonic nanosensors, Nat. Mater. 7 (6) (Jun. 2008) 442–453, https://doi.org/10.1038/nmat2162.

[42] R. de la Rica, M.M. Stevens, Plasmonic ELISA for the ultrasensitive detection of disease biomarkers with the naked eye, Nat. Nanotechnol. 7 (12) (Dec. 2012) 821–824, https://doi.org/10.1038/nnano.2012.186.

[43] H.S. Wasan, et al., CA 19-9 as a biomarker in advanced pancreatic cancer patients randomised to gemcitabine plus axitinib or gemcitabine alone, Br. J. Canc. 101 (7) (Oct. 2009) 1162–1167, https://doi.org/10.1038/sj.bjc.6605243.

[44] D. Gupta, C.G. Lis, Role of CA125 in predicting ovarian cancer survival - a review of the epidemiological literature, J. Ovarian Res. 2 (1) (09-Oct-2009) 13, https://doi.org/10.1186/1757-2215-2-13. BioMed Central.

[45] S. Kreth, M. Hübner, L.C. Hinske, MicroRNAs as clinical biomarkers and therapeutic tools in perioperative medicine, Anesth. Analg. 126 (2) (Feb. 2018) 670–681, https://doi.org/10.1213/ANE.0000000000002444.

[46] A. Agah, A. Hassibi, J.D. Plummer, P.B. Griffin, Design requirements for integrated biosensor arrays, Proc. *SPIE* 5699 (2005) 403–413, https://doi.org/10.1117/12.591300, 2005, vol. 5699, p. 403.

[47] J. Sun, et al., Uniform and reproducible plasmon-enhanced fluorescence substrate based on PMMA-coated, large-area Au@Ag nanorod arrays, Nano Res. 11 (2) (Feb. 2018) 953–965, https://doi.org/10.1007/s12274-017-1708-y.

[48] S. Park, et al., "Self-Assembly of nanoparticle-spiked pillar arrays for plasmonic biosensing, Adv. Funct. Mater. 29 (43) (Oct. 2019) 1904257, https://doi.org/10.1002/adfm.201904257.

[49] J. Pang, et al., Gold nanodisc arrays as near infrared metal-enhanced fluorescence platforms with tuneable enhancement factors, J. Mater. Chem. C 5 (4) (Jan. 2017) 917–925, https://doi.org/10.1039/C6TC04965F.

[50] J.S. Pang, et al., Tunable three-dimensional plasmonic arrays for large near-infrared fluorescence enhancement, ACS Appl. Mater. Interfaces 11 (26) (Jul. 2019) 23083–23092, https://doi.org/10.1021/acsami.9b08802.

[51] Z.A.R. Jawad, I.G. Theodorou, L.R. Jiao, F. Xie, Highly sensitive plasmonic detection of the pancreatic cancer biomarker CA 19-9, Sci. Rep. 7 (1) (Dec. 2017) 14309, https://doi.org/10.1038/s41598-017-14688-z.

[52] I.G. Theodorou, et al., Gold Nanostar Substrates for Metal-Enhanced Fluorescence through the First and Second Near-Infrared Windows, Chem. Mater. (2017), https://doi.org/10.1021/acs.chemmater.7b02313.

[53] B. Zhang, R.B. Kumar, H. Dai, B.J. Feldman, A plasmonic chip for biomarker discovery and diagnosis of type 1 diabetes, Nat. Med. 20 (8) (2014) 948–953, https://doi.org/10.1038/nm.3619.

[54] C. Hamon, et al., Collective plasmonic properties in few-layer gold nanorod supercrystals, ACS Photonics 2 (10) (Oct. 2015) 1482–1488, https://doi.org/10.1021/acsphotonics.5b00369.

[55] A. Centeno, N. Alford, F. Xie, Predicting the fluorescent enhancement rate by gold and silver nanospheres using finite-difference time-domain analysis, IET Nanobiotechnol. 7 (2) (Jun. 2013) 50–58, https://doi.org/10.1049/iet-nbt.2012.0016.

[56] F. Xie, A. Centeno, M.R. Ryan, D.J. Riley, N.M. Alford, Au nanostructures by colloidal lithography: from quenching to extensive fluorescence enhancement, J. Mater. Chem. B 1 (4) (Dec. 2013) 536–543, https://doi.org/10.1039/C2TB00278G.

[57] F. Xie, J.S. Pang, A. Centeno, M.P. Ryan, D.J. Riley, N.M. Alford, Nanoscale control of Ag nanostructures for plasmonic fluorescence enhancement of near-infrared dyes, Nano Res. 6 (7) (Jul. 2013) 496–510, https://doi.org/10.1007/s12274-013-0327-5.

[58] I.G. Theodorou, et al., Significant metal enhanced fluorescence of Ag 2 S quantum dots in the second near-infrared window, Nanoscale 8 (2016), https://doi.org/10.1039/c6nr03220f.

[59] F. Xie, M.S. Baker, E.M. Goldys, Homogeneous silver-coated nanoparticle substrates for enhanced fluorescence detection, J. Phys. Chem. B 110 (46) (2006) 23085–23091, https://doi.org/10.1021/jp062170p.

[60] A.S.D.S. Indrasekara, R. Thomas, L. Fabris, Plasmonic properties of regiospecific core-satellite assemblies of gold nanostars and nanospheres, Phys. Chem. Chem. Phys. 17 (2014) 33, https://doi.org/10.1039/c4cp04517c.

[61] A. Guerrero-Martínez, S. Barbosa, I. Pastoriza-Santos, L.M. Liz-Marzán, Nanostars shine bright for you: colloidal synthesis, properties and applications of branched metallic nanoparticles, Curr. Opin. Colloid Interface Sci. 16 (2) (Apr. 2011) 118–127, https://doi.org/10.1016/J.COCIS.2010.12.007.

[62] Hao Feng, Colleen L. Nehl, Jason H. Hafner, P. Nordlander*, Plasmon Resonances of a Gold Nanostar, Nano Lett. (2007), https://doi.org/10.1021/NL062969C.

[63] B. Liu, et al., High performance, multiplexed lung cancer biomarker detection on a plasmonic gold chip, Adv. Funct. Mater. 26 (44) (Nov. 2016) 7994–8002, https://doi.org/10.1002/adfm.201603547.

[64] S.M. Tabakman, et al., Plasmonic substrates for multiplexed protein microarrays with femtomolar sensitivity and broad dynamic range, Nat. Commun. 2 (1) (2011), https://doi.org/10.1038/ncomms1477.

[65] X. Li, et al., Autoantibody profiling on a plasmonic nano-gold chip for the early detection of hypertensive, Proc. Natl. Acad. Sci. U. S. A. 114 (27) (Jul. 2017) 7089–7094, https://doi.org/10.1073/pnas.1621457114.

[66] C. Pomares, et al., Validation of IgG, IgM multiplex plasmonic gold platform in French clinical cohorts for the serodiagnosis and follow-up of Toxoplasma gondii infection, Diagn. Microbiol. Infect. Dis. 87 (3) (Mar. 2017) 213–218, https://doi.org/10.1016/j.diagmicrobio.2016.09.001.

[67] B. Zhang, et al., Diagnosis of Zika virus infection on a nanotechnology platform, Nat. Med. 23 (5) (May 2017) 548–550, https://doi.org/10.1038/nm.4302.

[68] X. Li, et al., Plasmonic gold chips for the diagnosis of Toxoplasma gondii, CMV, and rubella infections using saliva with serum detection precision, Eur. J. Clin. Microbiol. Infect. Dis. 38 (5) (May 2019) 883–890, https://doi.org/10.1007/s10096-019-03487-1.

[69] Q.T. Nguyen, R.Y. Tsien, "Fluorescence-guided surgery with live molecular navigation — a new cutting edge, Nat. Rev. Canc. 13 (9) (Sep. 2013) 653–662, https://doi.org/10.1038/nrc3566.

[70] F. Meric, et al., Positive surgical margins and ipsilateral breast tumor recurrence predict disease-specific survival after breast-conserving therapy, Cancer 97 (4) (Feb. 2003) 926–933, https://doi.org/10.1002/cncr.11222.

[71] I.D. Nagtegaal, P. Quirke, What is the role for the circumferential margin in the modern treatment of rectal cancer? J. Clin. Oncol. 26 (2) (10-Jan-2008) 303–312, https://doi.org/10.1200/JCO.2007.12.7027.

[72] H.J. Chalfin, et al., Impact of surgical margin status on prostate-cancer-specific mortality, BJU Int. 110 (11) (Dec. 2012) 1684–1689, https://doi.org/10.1111/j.1464-410X.2012.11371.x.

[73] R.J. Snijder, A. Brutel de la Rivière, H.J. Elbers, J.M. van den Bosch, Survival in resected stage I lung cancer with residual tumor at the bronchial resection margin, Ann. Thorac. Surg. 65 (1) (Jan. 1998) 212–216, https://doi.org/10.1016/s0003-4975(97)01114-4.

[74] H. Kasban, M.A.M. El-Bendary, D.H. Salama, A comparaitve study of medical imaging techniques, Int. J. Inf. Sci. Intell. Syst. 4 (2) (2015) 37–58.

[75] A.L. Vahrmeijer, M. Hutteman, J.R. van der Vorst, C.J.H. van de Velde, J.V. Frangioni, Image-guided cancer surgery using near-infrared fluorescence, Nat. Rev. Clin. Oncol. 10 (9) (Sep. 2013) 507–518, https://doi.org/10.1038/nrclinonc.2013.123.

[76] J.T.C. Liu, N. Sanai, Trends and challenges for the clinical adoption of fluorescence-guided surgery, J. Nucl. Med. 60 (6) (01-Jun-2019) 756–757, https://doi.org/10.2967/jnumed.119.226795. Society of Nuclear Medicine Inc.

[77] K.J. Sexton, Y. Zhao, S.C. Davis, S. Jiang, B.W. Pogue, Optimization of fluorescent imaging in the operating room through pulsed acquisition and gating to ambient background cycling, Biomed. Optic Express 8 (5) (May 2017) 2635, https://doi.org/10.1364/boe.8.002635.

[78] G.M. van Dam, et al., Intraoperative tumor-specific fluorescence imaging in ovarian cancer by folate receptor-α targeting: first in-human results, Nat. Med. 17 (10) (Oct. 2011) 1315–1319, https://doi.org/10.1038/nm.2472.

[79] C. Wang, W. Fan, Z. Zhang, Y. Wen, L. Xiong, X. Chen, "Advanced nanotechnology leading the way to multimodal imaging-guided precision surgical therapy, Adv. Mater. 31 (49) (Dec. 2019) 1904329, https://doi.org/10.1002/adma.201904329.

[80] M.F. Attia, N. Anton, J. Wallyn, Z. Omran, T.F. Vandamme, An overview of active and passive targeting strategies to improve the nanocarriers efficiency to tumour sites, J. Pharm. Pharmacol. 71 (8) (Aug. 2019) 1185–1198, https://doi.org/10.1111/jphp.13098.

[81] M. Li, W. Zhang, B. Wang, Y. Gao, Z. Song, Q.C. Zheng, Ligand-based targeted therapy: a novel strategy for hepatocellular carcinoma, Int. J. Nanomed. 11 (Oct. 2016) 5645–5669, https://doi.org/10.2147/IJN.S115727.

[82] J. Yoo, C. Park, G. Yi, D. Lee, H. Koo, Active targeting strategies using biological ligands for nanoparticle drug delivery systems, Cancers (Basel). 11 (5) (May 2019), https://doi.org/10.3390/cancers11050640.

[83] C. Li, Q. Wang, Challenges and opportunities for intravital near-infrared fluorescence imaging technology in the second transparency window, ACS Nano (2018), https://doi.org/10.1021/acsnano.8b07536.

[84] W. Deng, F. Xie, H.T.M.C.M. Baltar, E.M. Goldys, Metal-enhanced fluorescence in the life sciences: here, now and beyond, Phys. Chem. Chem. Phys. 15 (38) (Sep. 2013) 15695, https://doi.org/10.1039/c3cp50206f.

[85] I.G. Theodorou, et al., Fluorescence enhancement from single gold nanostars: towards ultra-bright emission in the first and second near-infrared biological windows, Nanoscale 10 (33) (Aug. 2018) 15854–15864, https://doi.org/10.1039/C8NR04567D.

[86] C. Ayala-Orozco, et al., Fluorescence enhancement of molecules inside a gold nanomatryoshka, Nano Lett. 14 (5) (May 2014) 2926–2933, https://doi.org/10.1021/nl501027j.

[87] S. Xu, et al., "Gold nanobipyramids as dual-functional substrates for in situ 'turn on' analyzing intracellular telomerase activity based on target-triggered plasmon-enhanced fluorescence, ACS Appl. Mater. Interfaces 10 (32) (Aug. 2018) 26851–26858, https://doi.org/10.1021/acsami.8b05447.

[88] J. Sun, et al., "Ultrasensitive 'FRET-SEF' probe for sensing and imaging MicroRNAs in living cells based on gold nanoconjugates, Anal. Chem. 90 (5) (Mar. 2018) 3099–3108, https://doi.org/10.1021/acs.analchem.7b04051.

[89] Y. Luo, et al., Visualization of endogenous hydrogen sulfide in living cells based on Au nanorods@silica enhanced fluorescence, Anal. Chim. Acta 1053 (Apr. 2019) 81–88, https://doi.org/10.1016/j.aca.2018.12.008.
[90] M. Yu, et al., Metal-Enhanced Near Infrared Fluorescence-Based Sensor with Highly Improved Sensitivity for Adenosine Triphosphate,, ACS Appl. Nano Mater. (2018), https://doi.org/10.1021/acsanm.8b01583.
[91] T.A. Johnson, H.A. Jinnah, N. Kamatani, Shortage of cellular ATP as a cause of diseases and strategies to enhance ATP, Front. Pharmacol. 10 (Feb, 2019), https://doi.org/10.3389/fphar.2019.00098.
[92] Y.K. Xu, S. Hwang, S. Kim, J.Y. Chen, Two orders of magnitude fluorescence enhancement of aluminum phthalocyanines by gold nanocubes: a remarkable improvement for cancer cell imaging and detection, ACS Appl. Mater. Interfaces 6 (8) (Apr. 2014) 5619–5628, https://doi.org/10.1021/am500106c.
[93] I.G. Theodorou, et al., Towards multiplexed near-infrared cellular imaging using gold nanostar arrays with tunable fluorescence enhancement, Nanoscale 11 (4) (Jan. 2019) 2079–2088, https://doi.org/10.1039/C8NR09409H.
[94] B. Koh, et al., Visible to near-infrared fluorescence enhanced cellular imaging on plasmonic gold chips, Small 12 (4) (Jan. 2016) 457–465, https://doi.org/10.1002/smll.201502182.
[95] P.M. Favi, et al., Shape and surface effects on the cytotoxicity of nanoparticles: gold nanospheres versus gold nanostars, J. Biomed. Mater. Res. 103 (11) (2015) 3449–3462, https://doi.org/10.1002/jbm.a.35491.
[96] N. Khlebtsov, L. Dykman, Biodistribution and toxicity of engineered gold nanoparticles: a review of in vitro and in vivo studies, Chem. Soc. Rev. 40 (3) (Mar-2011) 1647–1671, https://doi.org/10.1039/c0cs00018c.
[97] I. Takeuchi, S. Nobata, N. Oiri, K. Tomoda, K. Makino, Biodistribution and excretion of colloidal gold nanoparticles after intravenous injection: effects of particle size, Bio Med. Mater. Eng. 28 (3) (2017) 315–323, https://doi.org/10.3233/BME-171677.
[98] Z.V. Feng, et al., Impacts of gold nanoparticle charge and ligand type on surface binding and toxicity to Gram-negative and Gram-positive bacteria, Chem. Sci. 6 (9) (Jun. 2015) 5186–5196, https://doi.org/10.1039/c5sc00792e.
[99] T.J. Cho, R.I. MacCuspie, J. Gigault, J.M. Gorham, J.T. Elliott, V.A. Hackley, Highly stable positively charged dendron-encapsulated gold nanoparticles, Langmuir 30 (13) (Apr. 2014) 3883–3893, https://doi.org/10.1021/la5002013.
[100] N.M. Schaeublin, et al., Surface charge of gold nanoparticles mediates mechanism of toxicity, Nanoscale 3 (2) (Feb. 2011) 410–420, https://doi.org/10.1039/c0nr00478b.
[101] N.S.B. Rosli, A.A. Rahman, A.A. Aziz, S. Shamsuddin, Determining the size and concentration dependence of gold nanoparticles in vitro cytotoxicity (IC 50) test using WST-1 assay, in: AIP Conference Proceedings, vol. 1657, 2015, p. 60001, https://doi.org/10.1063/1.4915189.
[102] W. Gao, K. Xu, L. Ji, B. Tang, Effect of gold nanoparticles on glutathione depletion-induced hydrogen peroxide generation and apoptosis in HL7702 cells, Toxicol. Lett. 205 (1) (Aug. 2011) 86–95, https://doi.org/10.1016/j.toxlet.2011.05.1018.
[103] S.C. Gad, K.L. Sharp, C. Montgomery, J.D. Payne, G.P. Goodrich, Evaluation of the toxicity of intravenous delivery of auroshell particles (Gold-Silica Nanoshells), Int. J. Toxicol. 31 (6) (Nov. 2012) 584–594, https://doi.org/10.1177/1091581812465969.
[104] A.R. Rastinehad, et al., Gold nanoshell-localized photothermal ablation of prostate tumors in a clinical pilot device study, Proc. Natl. Acad. Sci. U. S. A. 116 (37) (Sep. 2019) 18590–18596, https://doi.org/10.1073/pnas.1906929116.
[105] E. Blanco, H. Shen, M. Ferrari, Principles of nanoparticle design for overcoming biological barriers to drug delivery, Nat. Biotechnol. 33 (9) (08-Sep-2015) 941–951, https://doi.org/10.1038/nbt.3330. Nature Publishing Group.
[106] A.L. Bailly, et al., In vivo evaluation of safety, biodistribution and pharmacokinetics of laser-synthesized gold nanoparticles, Sci. Rep. 9 (1) (Dec. 2019), https://doi.org/10.1038/s41598-019-48748-3.
[107] D. Li, et al., “Excretable lanthanide nanoparticle for biomedical imaging and surgical navigation in the second near-infrared window, Adv. Sci. 6 (23) (Dec. 2019) 1902042, https://doi.org/10.1002/advs.201902042.